Laser-matter interaction in the bulk of a transparent solid: Confined microexplosion and void formation

Eugene G. Gamaly*
Laser Physics Centre, Research School of Physical Sciences and Engineering, the Australian National University, Canberra ACT 0200, Australia

Saulius Juodkazis,† Koichi Nishimura, and Hiroaki Misawa‡
CREST-JST and Research Institute for Electronic Science, Hokkaido University, N21-W10, CRIS Bldg., Kita-ku, Sapporo 001-0021, Japan

Barry Luther-Davies
Laser Physics Centre, Research School of Physical Sciences and Engineering, the Australian National University, Canberra ACT 0200, Australia

Ludovic Hallo, Philippe Nicolai, and Vladimir T. Tikhonchuk
Centre Lasers Intenses et Applications, UMR 5107 CEA CNRS - Université Bordeaux 1, 33405 Talence, Cedex, France
(Received 1 February 2006; revised manuscript received 8 April 2006; published 6 June 2006)

We present here the experimental and theoretical studies of a single femtosecond laser pulse interaction inside a bulk of transparent media (sapphire, glass, polymer). This interaction leads to the drastic transformations in a solid resulting in a void formation inside a dielectric. The laser pulse energy is absorbed within a volume of approximately 0.15 μm^3 creating a pressure and temperature comparable to that in the core of a strong multi-kilo-tons explosion. The material within this volume is rapidly atomized, ionized, and converted into a tiny super-hot dense cloud of expanding plasma that generates strong shock and rarefaction waves which result in the formation of a void, whose diameter is ~200 nm (for a 100 nJ pulse in sapphire). The way this structure forms can be understood from high-temperature plasma hydrodynamics. We demonstrate that unique states of matter characterized by temperatures $\sim 10^5$ K, heating rates up to the 10^{18} K/s, and pressures more than 100 times the strength of any material were created using a standard table-top laser in well-controlled laboratory conditions. We discuss the properties of the laser-affected solid and possible routes of laser-affected material transformation to the final state long after the pulse end. These studies will find application for the design of new materials and three-dimensional optical memory devices, and for formation of photonic band-gap crystals.

DOI: 10.1103/PhysRevB.73.214101 PACS number(s): 81.07.−b, 96.50.Fm, 62.50.+p, 47.40.Nm

I. INTRODUCTION

Recent studies demonstrated[1–8] that a single short laser pulse tightly focused inside the bulk of a transparent solid (silica glasses, crystalline quartz, sapphire, and polymers) could produce a cavity (void) confined in a pristine dielectric or in a crystal. Multiple pulses (high repetition rate lasers) can form three-dimensional structures with a controlled size less that half of a micrometer. To achieve this the laser beam must be focused into a volume less than λ^3 (where λ is the laser wavelength) using high numerical aperture optics. It has also been demonstrated that these structures can be formed in a different spatial arrangements.[3–8] This technique could be used for formation of photonic crystals, waveguides, and gratings for application in photonics. A single structure can also serve as a memory bit because it can be detected (read) by the action of a probe laser beam.[1]

There are different ways for inducing a change of properties in a bulk solid by laser irradiation. First, nondestructive and reversible phase transitions (photorefractive effect, color-centers, photodarkening in chalcogenide glasses, etc.) can be induced by lasers at the intensity below the damage threshold. Second, irreversible structural changes may be produced at high intensity above the optical breakdown threshold. We concentrate in this paper on the experimental and theoretical studies of the latter case for a high intensity.

There is a fundamental difference of the laser-matter interaction on the focusing conditions: either the laser beam is tightly focused inside a transparent material or it is focused onto the surface. In the former case the interaction zone containing high energy density is confined inside a cold and dense solid. For this reason the hydrodynamic expansion is insignificant, if the energy density is lower than the structural damage threshold, and above this threshold it is highly restricted. The deposition of high energy density in a small confined volume results in a change in the optical and structural properties in the affected region. As we demonstrate later, the unique conditions, extremely high pressure and temperature with record high heating and cooling rates, are created in the energy deposition region that may result in formation of new states of matter. Thereby one creates a zone that can be detected afterwards by an optical probe. If the structure is very small (much less than μm^3 in volume), it can be used as a memory bit for a high-density three-dimensional optical storage.

The interaction of a laser with matter at intensity above the ionization threshold proceeds in a way similar for all the materials.[9] The plasma generated in the focal region increases the absorption coefficient and produces a fast energy release in a very small volume. A strong shock wave is generated in the interaction region and this propagates into the surrounding cold material. The shock wave propagation is accompanied by compression of the solid material at the wave front and decompression behind it, leading to the formation of a void inside the material.

Transparent dielectrics have several distinctive features. First, they have a wide optical bandgap (it ranges from 2.2 to 2.4 eV for chalcogenide glasses and up to 8.8 eV for sapphire) that ensures the transparency in the visible or near infrared spectral range at low intensity. In order to induce material modification with moderate energy pulses, the laser intensity should be increased to induce a strongly nonlinear response from the material and to assure the plasma formation. This requires the intensities in excess of 10^{14} W/cm^2 where most dielectrics can be ionized early in the laser pulse.

A second feature of dielectrics is their relatively low thermal conductivity characterized by the thermal diffusion coefficient, η, which is typically $\sim 10^{-3}$ cm^2/s (compared with a few cm^2/s for metals). Therefore regions of a size l of a few microns will cool in a rather long time $t \sim l^2/\eta \sim 10$ μs. This opens an opportunity of a multi-pulse effect: the energy deposed by a sequence of several laser pulses focused into the same point in a dielectric will accumulate if the period between the pulses is shorter than the cooling time. Thus, if the single pulse energy is too low to produce any modification of the material, a change can be induced using a high pulse repetition rate because of this accumulation phenomenon.

The local temperature rise resulting from energy accumulation eventually saturates as the energy inflow from the laser is balanced by heat conduction, this typically taking a few thousand pulses at a repetition rate in the 10–100 MHz range. This effect has been experimentally demonstrated from measurements of the size of a void produced inside a dielectric by a high repetition rate laser.[2] The size of a damage zone increased with the number of pulses hitting the same point in the material. The accumulation effect has also been demonstrated during ablation of chalcogenide glass by a MHz repetition rate irradiation.[10] In the latter case, a single laser pulse heats the target surface only several tens of Kelvin, which is insufficient to produce any phase change. The energy density rises above the ablation threshold due to energy accumulation when a few hundred pulses hit the same spot. This is also accompanied by a marked change in the interaction physics from a laser-solid to a laser-plasma interaction. Thus repetition rate becomes another means to control the size of the structure produced by the laser.

In what follows we present first the experimental results on formation of a void inside a bulk transparent crystalline sapphire, silica, and polymer glasses (Sec. II). Then we describe the laser-solid interaction physics for the case where a laser beam is tightly focused inside a transparent dielectric at high intensity, well above the ablation threshold (Sec. III). We explain the physics of a void formation by a simple theory based on the energy and mass conservation that semiquantitatively complies with the experimental data (Sec. IV). Then we model the microexplosion by two-temperature plasma hydrodynamic computer simulations (Sec. V) and discuss the material modifications produced by the shock, heat, and rarefaction waves (Sec. VI). Then we demonstrate that the microexplosion is reduced copy of a macroscopic explosion producing huge temperature and pressure in well-controlled laboratory conditions (Sec. VII), discuss, and draw conclusions (Sec. VIII).

II. EXPERIMENTS

A. Laser focusing conditions

Amplified pulses from a femtosecond laser (Hurricane, Spectra Physics) were used for irradiation of dielectrics: a crystalline sapphire, silica glass (viosil), and polystyrene. The choice of very different materials from the point of view of their structural, mechanical, and optical properties was made in order to test the basic principles of nanovoid formation. Pulse energy necessary for the nanovoid formation in all these materials was typically smaller than 100 nJ (at focus) for the 200 fs pulse duration at the 800 nm wavelength. Single laser pulses were tightly focused inside a sample using an optical microscope (Olympus IX70) equipped with an oil-immersion objective lens of a numerical aperture NA $=1.35$. We define the focal volume as the one confined inside the surface where the intensity equals to a half of its maximum value[11] (for details see also Appendix A). The focal volume was approximately 0.15 μm^3 (it varied slightly with the refractive index), the beam waist radius was $r_{1/2}=0.26$ μm, and the focal area was $\pi r_{1/2}^2=0.21$ μm^2. Thus, the maximum average intensity at the waist of the focal area for a 100 fs, 100 nJ pulse reaches the value of 5×10^{14} W/cm^2. The corresponding peak laser power of 0.5 MW(for a 100 nJ pulse) was lower than the threshold for self-focusing in sapphire ($P_{cr}=1.9$ MW) and silica (2.0 MW) (see Appendix B and Ref. 12). Therefore, the laser energy could be delivered to the focal volume located from 5 to 50 μm below the crystal surface without inducing any damage in the region between the surface and the focus. In the case of polystyrene, the critical power of self-focusing was several orders smaller than that in sapphire and silica (see Appendix D). Hence, the presence of self-focusing was revealing itself in formation of a strongly elongated voids. It is noteworthy that the refractive index mismatch between the immersion oil ($n=1.52$), sapphire (1.75), silica (1.45), and polystyrene (1.55) had caused a strong dependence of the focal intensity distribution on the depth of irradiation due to spherical aberration (see Appendix B), especially for sapphire.

Since the mechanisms of the light-matter interactions in our experiments are highly nonlinear, the issues of precise measurement of pulse energy, duration, and intensity distribution at the focus were particularly addressed. It is especially important for the ultra-short (sub-ps) pulses. Calibration of the pulse energy measurement at the focus was carried out by solid-immersion lens;[13] the pulse duration and pulse prechirping were done by monitoring the frequency-resolved optical gating (FROG) after fs pulses passed

through the objective lens.[14] The FROG measurements were realized using a GRENOUILLE device.[15] It is noteworthy that the elaborated FROG trace measurements complied well with a simple procedure of monitoring the light-induced damage threshold using prechirping of pulse by compressor gratings (control of second-order dispersion). The smallest pulse energy at which the breakdown occurred corresponded to the shortest pulse at the focus. The smallest focusing depth (typically 5–10 μm) was used in measurements of laser irradiance in the focal plane. This allowed us to minimize the chromatic and, mainly, spherical aberrations of the focusing optics.

B. Examination of void in sapphire

An array of laser-affected spots aligned along the *c* axis ⟨0001⟩ inside the sapphire crystal was created by a sequence of single laser pulses. The pulse energy was chosen to be more than two times larger than the optically detectable damage threshold. The lateral and axial dimensions of the photomodified region were measured with a scanning electron microscope (SEM). For the lateral cross section, a focused ion beam milling was used to open the voids at their largest cross section by *in situ* examining the processed region with a SEM. For this purpose the voids were created at 5–7 μm depth. Figure 1 provides an overview of voids at the focal region. For an axial cross section the sample was cleaved along the *c* axis and examined with a SEM. The observed pattern is shown in Fig. 2(a). Careful examination revealed that the laser-affected region consists of a void surrounded by a shell extending to about twice the void diameter. This shell was identified as an amorphous sapphire by chemical etching since the amorphous sapphire should have a much higher solubility in the hydrofluoric acid compared with a crystalline material.[16] Indeed, the shell could be etched away completely using a 10% aqueous solution of hydrofluoric acid up to its smooth boundary with the pristine sapphire crystal as it can be seen in Fig. 2(b). This allowed us to measure the exact size of the laser-affected zone.

The dependence of the diameter of the laser-affected region on the pulse energy was measured at the same focusing conditions (Fig. 3). The central void only appears when the laser pulse energy at focus E_p was greater than 35 nJ. Below this threshold the laser-affected region extended to 250–300 nm, but the central void was absent. The gray region shows an amorphous compressed region. The size of the void and laser-affected region (amorphous material) can be expressed through the laser and material parameters using the laws of energy and mass conservation (see detailed explanation in Sec. IV). On this basis the curve 1 (Fig. 3) can be fitted by

$$D_v = l_a \sqrt[3]{A(E_p - E_{th,v})} \tag{1}$$

with the absorption depth $l_a = 100$ nm, the absorption coefficient $A = 0.6$, the pulse energy is in nJ, and the threshold energy for a void formation $E_{th,v} = 35$ nJ. Line 2 can be fitted by

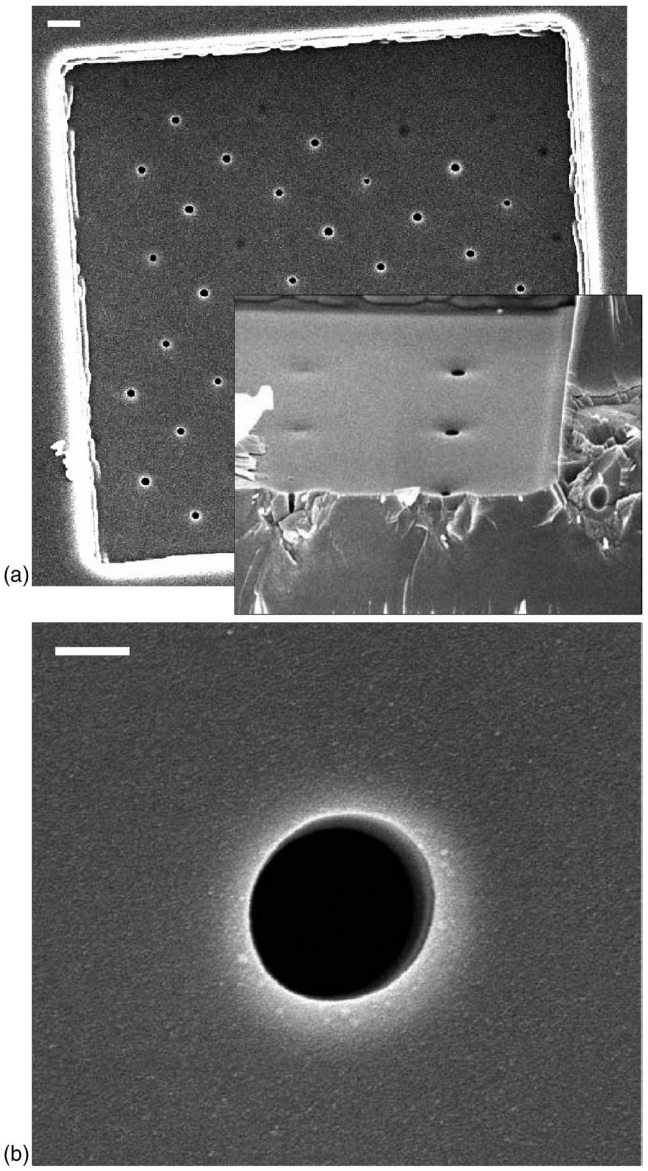

FIG. 1. SEM images of lateral cross sections of nanovoids in sapphire. (a) The voids were produced by single pulses of 100 nJ, 200 fs, 800 nm focused with an objective lens of NA=1.35. Focused ion beam (FIB) milling was used to slice at 6 μm depth over the voids. Inset shows a slanted view. (b) Single void; diameter 220 nm. Scale bars: 1 μm (a), 100 nm(b).

$$D_a = C l_a \sqrt[3]{A(E_p - E_{th,a})}, \tag{2}$$

where the threshold energy for formation of the amorphous region is $E_{th,a} = 21$ nJ and the factor $C = D_a/D_v = 1.85$, which is given by $C = 1/\sqrt[3]{(1 - 1/\delta)}$, accounts for the compression of the laser-affected region with the factor $\delta = 1.188$.

At the irradiation conditions below the threshold of void formation, a strong charging inside the amorphous part occurred during SEM imaging,[17] which implies the existence of a region of lower density in the region of highest laser intensity. The shape of the entire amorphous region becomes elliptical for higher pulse energies (Fig. 4). The strong dependence of the axial and lateral cross sections of the amorphous region on the depth presented in Fig. 4 cannot be

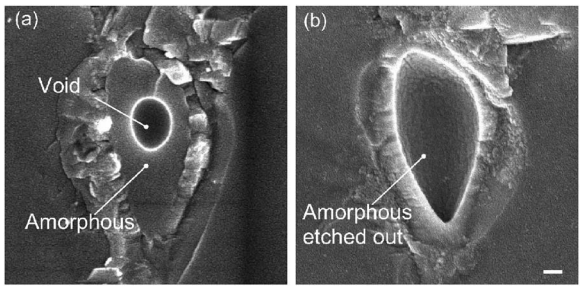

FIG. 2. SEM images of the axial cross section of the irradiated volume inside sapphire for the pulse energy of 100 nJ and the irradiation depth 20 μm. No cracks were observed in the irradiated sample. Scale bar: 100 nm.

explained by a spherical aberration alone. It can be accounted for by the Gaussian-to-Bessel pulse transformation without self-focusing as has been demonstrated recently,[18] i.e., an induced absorbtion at the highest intensity region on the optical axis leads toward self-action of the pulse and filamentation.[18,19] No cracks were observed in the crystal surrounding the laser-affected zone for pulse energies in the range 20–150 nJ. The onset of crack formation occurred at pulse energies larger than 170 nJ when the diameter of the amorphous region was larger than 600 nm. The effects of nonlinear propagation of the laser pulse above the threshold of self-focusing leads to complex filament and dot-like photo-modifications,[20,21] however these phenomena are out of the scope of this work.

C. Experiments with glasses and polystyrene

It follows from the above results that the size of the void and laser-affected area is inversely proportional to the cubic root of the Young's modulus of a material. Therefore, one would expect that experiments with glass (Y=75 GPa) and polystyrene (Y=3.5 GPa) should produce the bigger voids at the same absorbed energy, or lower thresholds for laser-induced changes. For this reason we studied nanovoid formation in silica glass (viosil) and polystyrene at the same irradiation conditions as for sapphire (Fig. 5). However, the threshold of optically detectable changes in glass was 13 nJ and the onset of void formation occurred at 30 nJ, that is, the threshold values are bigger than one may expect on the basis

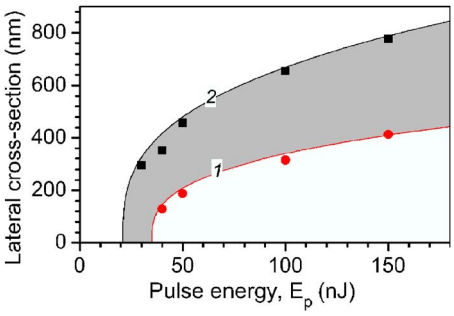

FIG. 3. (Color online) Lateral cross sections of the void 1 and amorphous region 2 versus the pulse energy at focus. Recording was carried out at the 30 μm depth. Gray region defines the domain affected by the shock.

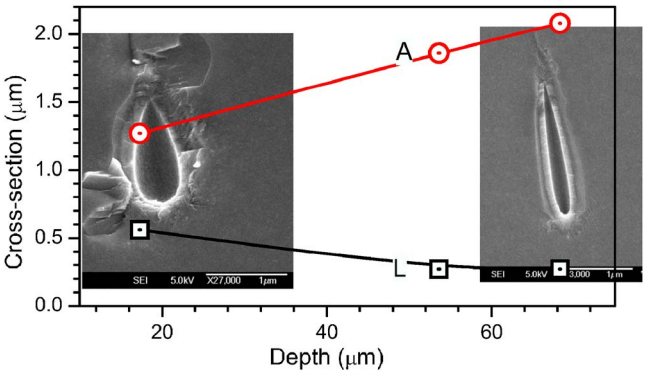

FIG. 4. (Color online) Dependence of the axial (A) and lateral (L) cross sections of the shock-affected region on the depth of irradiation. The pulse energy was 100 nJ. The amorphous part was etched out in a 10% aqueous solution of HF for 20 min. Inserts show the SEM images of the voids recorded at the depths 20 and 70 μm.

of a simple scaling. Similarly the voids in polystyrene were observed at pulse energy 10 nJ. We were unable to precisely determine the thresholds for optically detectable changes and void formation in the polystyrene due to the strong self-focusing, light scattering, and aberrations effects. Moreover, there is no optically distinctive boundary between laser-affected and pristine material in glass and polystyrene. It makes it difficult to apply the simple scaling based on the energy and mass conservation, which we used for interpretation of experiments with sapphire, to experiments with glasses and polystyrene where self-focusing, scattering, and aberrations are important. However, the voids formed in glass at pulse energies of 50 and 100 nJ were approximately 1.5 times larger than those in sapphire. Assuming the same absorption coefficient in both cases, such scaling is close to the expected 1.75 according to the ratio of Young's moduli, $\sqrt[3]{400/75} \simeq 1.75$.

To conclude this section we proved experimentally that the voids could be also created in glass and in polymer materials. The physical principles leading for the voids' formation are given in the following sections. Obviously, the final size, morphology, and shape of the void and its surroundings

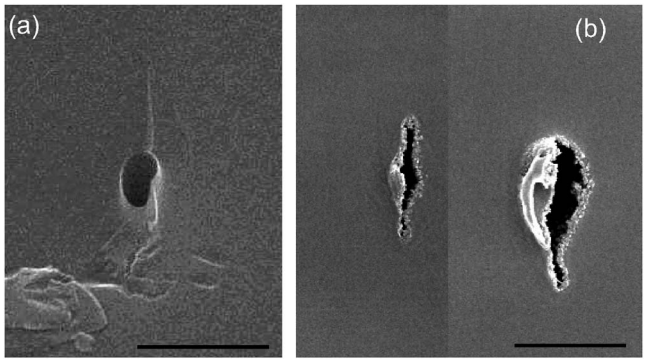

FIG. 5. SEM images of axial cross sections of voids in silica (viosil) at the pulse energy of 26 nJ (a) and in polystyrene at 11 and 17 nJ (b). Silica samples were cleaved; polystyrene was sliced by microtone. The irradiation depth 20 μm; the laser pulse arrives from above. Scale bars: 1 μm.

are affected by the relaxation and deexcitation of material, however the main parameters are qualitatively well (and in some cases quantitatively) described by the physics of the laser pulse triggered microexplosion. In what follows we present the results of the studies revealing the physical processes that occur in the laser-affected material during the pulse duration and after the pulse end.

III. LASER-MATTER INTERACTIONS INSIDE A BULK OF A SOLID AT HIGH INTENSITY

In order to produce some detectable structure inside the material one must transport the laser beam over a certain distance without losses and then deposit the energy in a small volume. That means that the absorption length should be large during a beam transport and the energy needs to be focused to the smallest possible volume, with dimensions of the order of the laser wavelength $\sim\lambda$ where the optical properties should be changed (absorption increased) under the laser action. Two particular properties of transparent dielectrics, the large absorption length and the low thermal conductivity, make them very suitable for that purpose.

The major mechanism of absorption in the low-intensity laser-solid interaction is the interband electron transition. Since the photon energy is smaller than the band-gap energy, the electron transitions are forbidden in linear approximation, which corresponds to a large real and small imaginary part of the dielectric function. The optical parameters in these conditions are only slightly changed during the interaction in comparison to those of the cold material. The absorption can be increased for shorter wavelengths where the photon energy becomes larger than the band-gap value or if the incident light intensity increases to the level where the multi-photon processes become important. We are interested in the second possibility. Under such conditions the properties of the material and the laser-material interaction change rapidly during the pulse. As the intensity increases above the ionization threshold, the neutral material transforms into plasma, which absorbs the incident light very efficiently. A localized deposition of the laser light creates a region of high energy density. A void in the bulk of material is created if the pressure in absorption volume significantly exceeds the Young's modulus of a solid. Multiple pulse action thereby allows a formation of various three-dimensional structures inside a transparent solid in a controllable and predictable way.

The full description of the laser-matter interaction process and laser-induced material modification from the first principles embraces the self-consistent set of equations that includes the Maxwell's equations for the laser field coupling with matter, complemented with the equations describing the evolution of energy distribution functions for electrons and phonons (ions) and the ionization state. A resolution of such a system of equations is a formidable task even for modern supercomputers. Therefore, the theoretical analysis is needed. This complicated problem is usually split into a sequence of simpler interconnected problems: the absorption of laser light, the ionization and energy transfer from electrons to ions, the heat conduction, and hydrodynamic expansion, which we are describing below.

A. Absorbed energy density

The absorbed laser energy per unit time and per unit volume, W_{abs}, is related to the divergence of the Pointing vector, $W_{abs}=-c\ \mathrm{div}\ \mathbf{E}\times\mathbf{H}/4\pi$. Time averaging over the laser period $2\pi/\omega$ and replacing the magnetic field from Maxwell's equations[22] results in the form

$$W_{abs}=\frac{\omega}{8\pi}\varepsilon''|E_a|^2, \tag{3}$$

where E_a is the electric field amplitude inside the medium and $\varepsilon=\varepsilon'+i\varepsilon''$ is the dielectric function. The spatial dependence of the field inside the solid is determined by the focusing conditions. One can see that Eq. (3) corresponds to the conventional Joule heating, $W_{abs}=\sigma' E_a^2$, taking into account the relation of the real part of the conductivity to the imaginary part of the dielectric function, $\sigma'=\omega\varepsilon''/4\pi$. The absorbed energy should be related to the incident laser flux intensity, $I=cE_0^2/4\pi$, where E_0 is the incident laser electric field. The value of the electric field at the solid-vacuum interface, $E_a(0)$, is related to the amplitude of the incident laser field by the boundary conditions:

$$|E_a(0)|^2=\frac{4}{|1+n+i\kappa|^2}E_0^2, \tag{4}$$

where $n+i\kappa=\sqrt{\varepsilon}$ is the complex index of refraction. Finally, the expression of the absorbed energy density through the incident laser flux reads

$$W_{abs}=\frac{\omega}{c}\frac{8n\kappa}{|1+n+i\kappa|^2}I\equiv\frac{A}{l_{abs}}I, \tag{5}$$

where $l_{abs}=c/(2\omega\kappa)$ is the intensity decay length and A is the absorption coefficient defined by the Fresnel formula[22]

$$A=1-R=\frac{4n}{(n+1)^2+\kappa^2}. \tag{6}$$

The electric field exponentially decays inside a focal volume, $E=E_a(0)\exp(-x/2l_{abs})$. It was implicitly assumed in this derivation that the optical parameters of the medium are space and time independent and that they are not affected by laser-matter interaction. One also should note that the relations between the Pointing vector, intensity, and absorption presented above are rigorously valid only for the plane wave. However, comparison with experiments has shown that they are also valid with sufficient accuracy for tightly focused beams as well.

Duration of a typical pulse of $\sim$100 fs is shorter than the electron-phonon and electron-ion collision times as we show later in the paper. Therefore the electron energy distribution during the pulse time has a delta-function-like shape peaked near the energy that can be estimated from the general formula of Joule heating (5) under assumption that the spatial intensity distribution inside a solid and material parameters are time independent. We denote the energy per single electron by ϵ_e (it should not be confused with the dielectric function ε). Then the electron energy density change in accordance with (5) reads

$$\frac{d(n_e\epsilon_e)}{dt} = \frac{A}{l_{abs}} I(t). \tag{7}$$

Correspondingly the single electron energy grows with time during the pulse as follows:

$$\epsilon_e = \frac{A}{n_e l_{abs}} \int_0^t I(t)dt. \tag{8}$$

The electron energy gained to the end of the pulse of the duration t_p reads

$$\epsilon_e(t_p) = \frac{AF_p}{n_e l_{abs}} \equiv \frac{Q_{dep}}{n_e}, \tag{9}$$

where $F_p = \int_0^{t_p} I(t)dt$ is the laser fluence and Q_{dep} is the deposited laser energy per unit volume. The electron temperature rises to eV level during the pulse. The ionization of a solid occurs that affects the optical properties. Thus, the next step is to introduce the model where the optical properties are dependent on the changing electron number density and electron energy. Let us calculate first the electron energy gain rate.

B. Electron energy gain rate

The simplest model for the electron acceleration and subsequent electron transfer from the valence band to the conduction band applies if the energy gain rate by electron in a valence band exceeds all energy losses. Under the conditions of experiments in question the direct photon absorption by electrons in a valence band is small because the energy of the laser photon is smaller than a band gap, $\hbar\omega < \Delta_{gap}$. However, a few (seed) electrons can be always created by the multiphoton absorption. These electrons oscillate in the laser electromagnetic field and can be gradually accelerated to energy in excess of the band gap.

This is well-known model of free electron acceleration in a simple plasma, where absorption occurs due to electron collisions. Three-body interactions (collisions) involving photon, electron, and atom (ion) are responsible for the absorption. In a model of electron acceleration in the high-frequency field, all collisions are accounted for through the effective collision frequency that enters into the Newton equation of electron motion as a friction force. The response of electrons (the ions are considered as a neutralizing background) on the action of the applied high-frequency electric field is described by the following dielectric function:[23]

$$\varepsilon = 1 - \frac{\omega_p^2}{\omega(\omega + i\nu_{ef})}. \tag{10}$$

Here, the electron plasma frequency, $\omega_p = (4\pi e^2 n_e/m^*)^{1/2}$, is an explicit function of the number density of the conductivity electrons, n_e, and the electron effective mass, m^*. The heating rate expresses through the imaginary part of the dielectric function in accordance with Eq. (3):

$$Q_{abs} = \frac{n_e e^2 E^2 \nu_{ef}}{2m_e(\nu_{ef}^2 + \omega^2)} = n_e \nu_{ef} \frac{2\epsilon_{osc}\omega^2}{\nu_{ef}^2 + \omega^2}, \tag{11}$$

where $\epsilon_{osc} = m_e v_{osc}^2/4 = e^2E^2/4m_e\omega^2$ is the electron quiver energy. The average heating rate of a single electron as a function of the laser and material parameters now reads

$$\frac{d\epsilon_e}{dt} = \nu_{ef} \frac{2\epsilon_{osc}\omega^2}{\nu_{ef}^2 + \omega^2} \equiv \nu_{ef}\Delta\epsilon_e, \tag{12}$$

where $\Delta\epsilon_e$ is the energy gained by an electron in one collision.

C. Optical breakdown: Ionization mechanisms and thresholds

Optical breakdown of dielectrics and optical damage produced by the action of an intense laser beam has been extensively studied over the several decades.[23–35] It is well established[23–26] that two major mechanisms are responsible for conversion of a neutral material into plasma: the ionization by the electron impact (avalanche ionization), and the ionization produced by simultaneous absorption of multiple photons.[36] The relative contribution of both mechanisms depends on the laser wavelength, pulse duration, intensity, and the atomic number. We present here simple analytic estimates of the breakdown threshold and the transient number density of electrons created in the absorption region.

1. Ionization by the electron impact (avalanche ionization)

Under the conditions of the experiments in question the probability of a direct photon absorption by electrons in the valence band is small. However, a few (seed) electrons can be always found in the conduction band. These electrons oscillate in the laser electromagnetic field and can be gradually accelerated to the energy in excess of the band gap. Electrons with $\epsilon_e > \Delta_{gap}$ collide with electrons in the valence band and can transfer a sufficient energy to them for the excitation into the conduction band. Thus the number of free electrons increases, which provokes the effect of avalanche ionization. The probability of such an event per unit time can be estimated with the help of (12) as follows:

$$w_{imp} \approx \frac{1}{\Delta_{gap}} \frac{d\epsilon_e}{dt} = \nu_{ef} \frac{\Delta\epsilon_e}{\Delta_{gap}}. \tag{13}$$

In this simplified approach the electron is accelerated continuously and the probability of ionization is proportional to the electron oscillation energy and it depends on the electron-phonon collision frequency, ν_{ef}. The electron (hole)-phonon momentum exchange rate depends on the temperatures of the electrons and phonons. At low intensities the electron temperature just exceeds the Debye temperature and the electron-phonon collision rate increases in proportion to the temperature. For SiO_2 the effective collision frequency ν_{ef} is of the order of 5×10^{14} s^{-1}[26] and it is smaller than the light frequency, $\omega \gtrsim 10^{15}$ s^{-1}. It follows from (13) that the ionization rate then grows in proportion to the square of the laser wavelength in correspondence with the Monte Carlo solutions to the Boltzmann kinetic equation for electrons.[26] With further increase in temperature, the effective electron-lattice collision rate responsible for momentum exchange saturates at the plasma frequency ($\sim 10^{16}$ s^{-1}).[9,37] At this stage the wavelength dependence of the ionization rate almost disappears as $\omega < \nu_{ef}$, according to Eq. (13). This con-

clusion is in agreement with the rigorous calculations of Ref. 26.

It is worth noting that the classical (as opposed to quantum) treatment is valid for very high intensity and the laser wavelength of a few hundred nm. It was established[23] that the value of the dimensionless parameter $\Gamma=\epsilon_e\Delta\epsilon_e/(\hbar\omega)^2 \sim 1$ separates the parameter space into two regions where the classical, $\Gamma>1$, or quantum, $\Gamma<1$, approach is valid. Thus, if the electron energy gain in one collision, $\Delta\epsilon_e\sim\epsilon_{osc}$, and the electron energy ϵ_e are both higher than the photon energy, then $\Gamma>1$ and the classical equations (12) and (13) are valid. The classical approach applies at high laser intensities that have been recently used in short-pulse-solid interaction experiments. For example, at $I=10^{14}$ W/cm^2 and $\hbar\omega=2-3$ eV, one has $\Delta\epsilon_e/\hbar\omega\sim 3-4$, $\epsilon_e>\Delta\epsilon_e$, therefore, $\Gamma\gg 1$ and the classical approximation applies.

2. Multi-photon ionization

The second ionization mechanism relates to simultaneous absorption of several photons.[36,38] This process has no threshold and hence the contribution of multi-photon ionization can be important even at relatively low intensity. Multi-photon ionization creates the initial (seed) electron density, which then grows by the avalanche process. The multi-photon ionization can proceed in two limits separated by the value of the Keldysh parameter $\Gamma=\epsilon_{osc}/\Delta_{gap}\sim 1$. The tunneling ionization occurs under the condition where $\Delta_{gap}\ll\epsilon_{osc}$. The ionization probability in this case does not depend on the frequency of field and it is similar to the action of a static field.[36,38,39]

The multi-quantum photo-effect takes place in the opposite limit $\Delta_{gap}>\epsilon_{osc}$. The intensities around $I\sim 10^{14}$ W/cm^2 and photon energy $\hbar\omega=2-3$ eV are typical for subpicosecond pulse interaction experiments with the fused silica.[27–35] The Keldysh parameter for all recently published experiments is around unity, depending on the band-gap value (for some materials such as silicon, it is higher, for silica it is lower than unity). Therefore it is reasonable to take the ionization probability (probability of ionization per atom per second) in the multi-photon form:[23]

$$w_{mpi}\approx\omega n_{ph}^{3/2}\left(\frac{\epsilon_{osc}}{2\Delta_{gap}}\right)^{n_{ph}}, \tag{14}$$

where $n_{ph}=\Delta_{gap}/\hbar\omega$ is the number of photons necessary for the electron to be transferred from the valence to the conduction band. One can see that with the near band-gap energy, $\Delta_{gap}\sim\hbar\omega$, and $\epsilon_{osc}\sim\Delta_{gap}$, both Eqs. (14) and (13) give the ionization rate of 10^{15} s^{-1}, thus ionization time is much shorter than the laser pulse duration.

The multi-photon ionization is important at low intensities where the avalanche process dominates. It generates the initial number of electrons, which, although small, can be multiplied by the avalanche process. The multi-photon ionization rate dominates, $w_{mpi}>w_{imp}$, for any relationship between the frequency of the incident light and the effective collision frequency in conditions when $\epsilon_{osc}>\Delta_{gap}\sim\hbar\omega$. However, even at high intensity the contribution of the avalanche process is crucially important: at $w_{mpi}\sim w_{imp}$ the seed electrons are generated by multi-photon effect, while final growth is due to the avalanche ionization. Such an interplay of two mechanisms has been demonstrated with the direct numerical solution to the kinetic Fokker-Planck equation.[28] Under conditions $w_{mpi}\sim w_{imp}\sim 10^{15}$ s^{-1} ($\epsilon_{osc}\sim\Delta_{gap}\sim\hbar\omega$) the critical density of electrons is achieved in a few fs.

Let us note that the collisional (avalanche) ionization plays a more important role in the solid dielectrics in comparison to that in gases. The multi-photon process in gases never leads to a complete ionization due to the screening of the laser electric field by the electrons produced in the ionization process. The multi-photon ionization rate nonlinearly depends on the electric field intensity, thus even small screening produces a strong reduction of the ionization probability. In a solid the avalanche ionization prevails over multi-photon process, because the electrons heating rate is proportional to the electric field intensity and therefore is less sensitive to the screening effect. Penano *et al.* demonstrated recently this effect in 1D calculations accounting for both, the field and collisional ionization.[40] They show that the ionization is completed within 100 fs due to the only collisional effect. It is also shown for the fluences above 5–6 J/cm^2 the ionization is complete early in the pulse. Therefore for pulse duration ~100 fs the ionization threshold can be reached early in the pulse and afterwards the interaction proceeds in the laser-plasma interaction mode.

D. Ionization thresholds

It is generally accepted that the breakdown occurs when the number density of electrons reaches the critical density corresponding to the frequency of the incident light $n_c=m_e\omega^2/4\pi e^2$. Thus, the laser parameters (intensity, wavelength, pulse duration) and the material parameters (band-gap width and electron-phonon effective collision rate) at the breakdown threshold are combined by condition, $n_e=n_c$.

The ionization threshold for the majority of transparent solids lies at intensities between 10^{13} and 10^{14} W/cm^2 for $\lambda\sim 1$ μm with a strong nonlinear dependence on intensity. The conduction-band electrons gain energy in an intense short pulse much faster than they transfer energy to the lattice. Therefore the actual structural damage (breaking interatomic bonds) occurs after the electron-to-lattice energy transfer, usually after the pulse end. It was determined that in the fused silica the ionization threshold was reached to the end of a 100 fs pulse at 1064 nm at the intensity 1.2×10^{13} W/cm^2.[26] Similar breakdown thresholds in a range of $(2.8\pm 1)\times 10^{13}$ W/cm^2 were measured in interaction of a 120 fs, 620 nm laser with the glass, MgF_2, sapphire, and fused silica.[29] This behavior is to be expected, since all transparent dielectrics share the same general properties of slow thermal diffusion, fast electron-phonon scattering, and similar ionization rates. The breakdown threshold fluence F_p is an appropriate parameter for characterization of ionization conditions as a function of the pulse duration. It is found that the threshold fluence varies slowly for pulse durations below 100 fs. For example, for the most studied case of fused silica, the following threshold fluences were determined: ~2 J/cm^2 at 1053 nm, ~300 fs, and ~1 J/cm^2 at 526 nm,

~200 fs;[28] 1.2 J/cm^2 at 620 nm, ~120 fs;[29] 2.25 J/cm^2 at 780 nm, ~220 fs;[32] and 3 J/cm^2 at 800 nm;10–100 fs.[33]

E. Ionization state to the end of the laser pulse

Let us estimate first the electron number density generated by the ionization processes to the end of the laser pulse with recombination taken into account. In dense plasmas the recombination proceeds mainly by three-body collisions with one electron acting as a third body.[41] Then the equation for the electron density reads

$$\frac{dn_e}{dt} = w_{ion} n_e - \beta_e n_i n_e^2, \tag{15}$$

where $w_{ion} = \max\{w_{imp}, w_{mpi}\} \sim 10^{15}$ s^{-1} is the ionization rate and β_e is the recombination rate:

$$\beta_e = 8.75 \times 10^{-27} Z^2 \epsilon_e^{-9/2} \ln \Lambda. \tag{16}$$

Here, the electron energy is in eV, Z is the average ion charge, and $\ln \Lambda$ is the Coulomb logarithm.[41] One can see that ionization time, $t_{ion} \sim w_{ion}^{-1}$, and recombination time $t_{rec} \approx 1/\beta_e n_e^2$, are of the same order of magnitude, ~1 fs, and both are much shorter then the pulse duration. Therefore, the electron number density to the end of the pulse can be estimated in the stationary approximation as follows: $n_e^2 \approx w_{ion}/\beta_e$. Taking $\epsilon_e \sim 50$ eV (as calculated below in Sec. III H), $Z=5$, and $\ln \Lambda \sim 2$, one obtains that $n_e \sim 3.3 \times 10^{23}$ cm^{-3}. This is a clear indication of the ionization equilibrium, and that the multiple ionizations take place. We take that into account in the next section.

F. Ionization after the pulse end

The electron temperature at the end of the pulse is much higher than the ionization potential. Therefore, the ionization by the electron impact continues after the pulse end. The evolution of the electron number density can be calculated from the equation similar to (15) by taking into account the ionization and recombination processes:[41]

$$\frac{dn_e}{dt} \approx \alpha_e n_e n_a - \beta_e n_i n_e^2, \tag{17}$$

where $\alpha_e = \sigma_e v_e (J_Z/\epsilon_e + 2)\exp(-J_Z/\epsilon_e)$ is the impact ionization rate, $v_e = \sqrt{2\epsilon_e/m_e}$ is the electron velocity, J_Z is the ionization potential, and $\sigma_e \simeq 2 \times 10^{-16}$ cm^2 is the effective cross section of the electron-ion collision. For parameters of the experiments in question $\epsilon_e \sim 50$ eV (as calculated below in Sec. III H) and the time for establishing the ionization equilibrium is very short, $\tau_{eq} \approx 1/\alpha_e n_e \sim 0.1$ fs. Then the average charge of multiply ionized ions can be estimated assuming the equilibrium conditions and applying the principle of detailed balance.[41]

G. Laser-modified optical properties of the ionized solid

As it was demonstrated above, the ionization is completed and the electron number density is saturated in a few fs early in the beginning of the laser pulse. The plasma in the focal volume has a free-electron density comparable to the ion density of about 10^{23} cm^{-3}. Hence, the laser interaction proceeds with a plasma during the remaining part of the pulse. One can consider the electron number density (and thus the electron plasma frequency) as being constant and estimate the optical properties of laser-affected solid from Eq. (10), taking into account the fact that the effective collision frequency in this dense nonideal plasma is approximately equal to the plasma frequency, $\nu_{ef} \sim \omega_p$.[9,37]

For example, the optical parameters of plasma obtained after the breakdown of a silica glass by an 800 nm laser ($\omega = 2.4 \times 10^{15}$ s^{-1}) are as the follows: $\omega_p = 1.45 \times 10^{16}$ s^{-1}, $\varepsilon' = 0.105$, $\varepsilon'' = 2.79$, and correspondingly $n = 1.20$ and $\kappa = 1.16$. Then the absorption length $l_{abs} = 54$ nm and absorption coefficient $A = 0.77$. Therefore, the optical breakdown and further heating convert silica into a metal-like medium, reducing the energy deposition volume by two orders of magnitude and correspondingly massively increasing the absorbed energy density.

H. Average ion charge, electron energy, and pressure in the focal region at the laser pulse end

Let us estimate the average electron temperature T_e in a silica glass at the pulse end by considering the ionization potential J_Z and the energy loss for ionization as continuous functions of the average ion charge $Z = n_e/n_i$.[41] Then the electron thermal energy is the difference of the deposited energy, $Q_{dep} = AF_p/l_{abs}$ (9), and the ionization losses:

$$n_e T_e = Q_{dep} - n_{SiO_2}(Q_Z^{Si} + 2Q_Z^{O}), \tag{18}$$

where $n_e = 3Z n_{SiO_2}$ is the electron density and $Q_Z^{Si,O}$ is the energy needed for ionization of the correspondent ion species to the charge Z. The average charge Z depends on the electron temperature through the Saha equation:[41]

$$J_{Z+1/2} = T_e \ln(a T_e^{3/2}/n_e), \tag{19}$$

where $a = 6 \times 10^{21}$ cm^{-3}eV$^{-3/2}$, the electron temperature is in eV, and the electron density in cm^{-3}. The set of Eqs. (18) and (19) has been solved numerically with the ionization potentials for silicon and oxygen presented in Appendix C. Taking for the laser absorption the estimates obtained above, $l_{abs} = 54$ nm, $F_p = 14.9$ J/cm^2, and $A = 0.77$, one obtains $Q_{dep} = 4.25$ MJ/cm^3, $Z_{Si} = 5$, $Z_O = 4.5$, $n_e = 3 \times 10^{23}$ cm^{-3}, and $T_e \simeq 50$ eV. Thus the electron pressure $P_0 = P_e = n_e T_e$ to the pulse end comprises 2.7 TPa.

I. Energy transfer from electrons to ions

The hydrodynamic motion can start after the electrons transfer the absorbed energy to ions. The following processes are responsible for the energy transfer from electrons to ions: recombination, electron-to-ion energy transfer in Coulomb collisions, ion acceleration in the field of charge separation (gradient of electronic pressure), and electronic heat conduction. We already accounted for the recombination. Below we compare the characteristic times of other processes.

1. Electron-to-ion energy transfer by Coulomb collisions

The electron-to-ion energy exchange rate in plasma, ν_{en}, is proportional to the electron-ion mass ratio, m_e/m_i, and it is

expressed via the electron-ion momentum exchange rate, ν_{ei}, in accordance with Ref. 42 as follows:

$$\nu_{en} \approx 2\frac{m_e}{m_i}\nu_{ei}. \tag{20}$$

The Coulomb forces dominate the interactions between the charged particles in the dense plasma created in our experiments to the end of the pulse. The parameter that characterizes the plasma state is the number of particles in the Debye sphere $N_D = 1.7\times 10^9\sqrt{T_e^3/n_e}$ (Ref. 42), where T_e is in eV and n_e is in cm^{-3}. A plasma is in an ideal state if $N_D \gg 1$. In a plasma with parameters estimated above ($Z=5$, $\ln\Lambda = 1.7$, $n_e = 3\times 10^{23}\ \mathrm{cm}^{-3}$, $T_e = 50$ eV), N_D is of the order of unity, which is a clear signature of the nonideal conditions. The maximum value for the electron-ion momentum exchange rate in nonideal plasma approximately equals the plasma frequency, $\nu_{ei} \sim \omega_{pe} \sim 10^{16}\ \mathrm{s}^{-1}$.[9,37] Hence electrons in ionized fused silica ($m_i = 3.32\times 10^{-23}$ g) transfer the energy to ions over a time $t_{en} = \nu_{en}^{-1}$ of a few ps.

2. Ion acceleration by the gradient of the electron pressure

Let us estimate the time for the energy transfer from electrons to ions under the action of electronic pressure, $P_e = n_e T_e$, assuming that ions are initially cold. The Newton equation for ions reads

$$\frac{\partial(m_i n_i u_i)}{\partial t} \approx -\nabla P_e.$$

The kinetic velocity of ions ($Zn_i \approx n_e$) then estimates as follows:

$$u_i \approx \frac{ZT_e t}{m_i l_{abs}}. \tag{21}$$

The time for the energy transfer from electrons to ions is defined by the condition that the ions kinetic energy compares to that of electrons, $\frac{1}{2}m_i u_i^2 \sim T_e$. Then from Eq. (21) one obtains the energy transfer time by the action of the electrostatic field of charge separation:

$$t_{el\ st} \sim \frac{l_{abs}}{Z}\left(\frac{2m_i}{T_e}\right)^{1/2}. \tag{22}$$

For the parameters mentioned above this time is of the same order of a few ps as t_{en} (20). These estimates define the time when the laser-deposited energy is transferred to ions and the hydrodynamic expansion commences. Moreover, the estimate below shows that during this time the deposited energy is confined in the volume of absorption and does not spread over by transport processes.

3. Electronic heat conduction

Unlike motion of the ions, energy transfer by nonlinear electronic heat conduction starts immediately after the energy absorption. Therefore a heat wave can propagate outside of heated area before the shock wave emerges. The thermal diffusion coefficient is defined conventionally as the following:

$$\eta = \frac{v_e^2}{3\nu_{ei}}. \tag{23}$$

The characteristic cooling time of the hot region of the size l_{abs} is defined as follows: $t_{cool} = l_{abs}^2/\eta$. For the conditions of the experiments in question, $\nu_{ei} \sim 10^{16}\ \mathrm{s}^{-1}$ and $T_e = 50$ eV, the diffusion coefficient $\eta \sim 1\ \mathrm{cm}^2/\mathrm{s}$ and the cooling time is $t_{cool} \approx 15$ ps, which is much longer than the electron-ion exchange time.

Summing up the results of this section we shall note that in the dense plasma created by the tight focusing inside a bulk solid the major processes responsible for the electron-to-ion energy transfer are different from those in the laser ablation. The fastest process of the energy transfer from hot electrons to the ions is the electron-ion recombination by three-body collisions with one electron acting as a third body. This process takes ~ 1 fs. The ion acceleration by the gradient of the electron pressure and the electron-to-ion energy transfer by the Coulomb collisions both comprise ~ 1 ps. This is the time of hydrodynamic motion. The electronic nonlinear heat conduction becomes important much later, about 15 ps after the pulse end.

IV. SHOCK WAVE FORMATION, PROPAGATION, AND STOPPING

We present in this section a qualitative picture of hydrodynamic motion that emerges after the laser pulse end. That complements the results of more detailed computer hydrodynamic modeling that we present later on in Sec. V. For our estimates we consider the silica glass instead of a crystalline material due to its isotropic optical and mechanical properties.

A. Shock wave formation

The hydrodynamic motion starts, that is, the shock wave emerges from the energy deposition zone, when the electrons have transferred their energy to ions. As we have shown above, that process takes a few ps. In this time scale the total deposited energy, $Q_{dep} = 2.7\ \mathrm{MJ/cm}^3$, builds up the pressure that drives the shock wave. This pressure, $P_0 \approx 2.7$ TPa, considerably exceeds the Young's modulus for the majority of materials (for example, $Y = 400$ GPa for the sapphire and 75 GPa for the cold silica). Therefore, a strong shock wave emerges that compresses the material up to the density $\rho \simeq \rho_0(\gamma+1)/(\gamma-1)$. This corresponds to $\rho_{max} \simeq 2\rho_0$ as the adiabatic constant γ for the majority of cold solids is ~ 3.

The compressed material behind the shock wave front can then be transformed to another phase state in such high-pressure conditions. After unloading the shock-affected material undergoes transformation into a final state at normal pressure. The final state may possess properties different from those in the initial state. We consider in succession the stages of compression and phase transformation, pressure release, and material transformation into a postshock state.

B. Shock wave expansion and stopping

The shock wave propagating in a cold material loses its energy due to dissipation, and it gradually transforms into the

sound wave due to the work done against the internal pressure (Young's modulus, Y) that resists material compression. Let us consider for simplicity a spherically symmetric motion. The distance at which the shock front effectively stops defines the shock-affected volume. Actually at this point the shock wave converts into a sound wave, which propagates further into the material without inducing any permanent changes to a solid. This stopping distance, r_{stop}, can be estimated from the condition[41] that the internal energy in the volume inside the shock front is comparable to the absorbed pulse energy: $\frac{4}{3}\pi Y r_{stop}^3 \approx E_{abs}$. Then the stopping distance reads

$$r_{stop} \approx \sqrt[3]{\frac{E_{abs}}{\frac{4}{3}\pi Y}}. \tag{24}$$

In other words, at this position the pressure behind the shock front equals the internal pressure of the cold material. One can reasonably suggest that the sharp boundary observed between the amorphous (laser-affected) and crystalline (pristine) sapphire in the experiments corresponds to the distance where the shock wave effectively stopped. The experimentally measured dependence of the laser-affected zone diameter D_a (the outer size of amorphous region) on the laser energy (1) agrees rather well with Eq. (24) by attributing $D_a \approx 2r_{stop}$ and $E_{abs}=AE_p$. Then, measuring E_{abs} in nJ, we deduce for l_a the value of 80 nm. This characteristic length is, in fact, very close to the absorption depth ($l_{abs}=54$ nm) as calculated above. The sound wave continues to propagate at $r > r_{stop}$, apparently not affecting the properties of material.

C. Rarefaction wave: Formation of void

The experimentally observed formation of a hollow, or low-density, region within the laser-affected volume, the void, can be understood from the simple reasoning. Let us again consider for simplicity spherically symmetric motion. The strong spherical shock wave starts to propagate outside the center of symmetry, compressing the material. At the same time, behind the shock front, a rarefaction wave propagates to the center of the sphere, creating a void. One can apply the mass conservation law to estimate the density of compressed material from the void size. Indeed, the mass conservation relates the size of the void to compression of the surrounding shell. One can use the void size from the experiments and deduce the compression of the surrounding material. The void formation inside a solid is only possible if the mass initially contained in the volume of the void was pushed out and compressed. Thus after the microexplosion the whole mass initially confined in a volume with radius r_{stop} resides in a layer in between r_{stop} and r_v, which has a density $\rho=\rho_0\delta$ with a compression factor $\delta > 1$. The void radius can be expressed through the compression ratio $C=(1-1/\delta)^{-1/3}$, and the radius of the laser-affected zone with the help of the mass conservation as follows:

$$r_v = r_{stop}/C, \tag{25}$$

which serves as justification and basis for the interpolation formula (2). Typically we observed $r_v \sim 0.5 \times r_{stop}$, which means that amorphous material shall have a density 1.14 times higher than that of crystalline sapphire. Note that this is a void size *immediately after the interaction*; the final void forms after the reverse phase transition and cooling.

V. HYDRODYNAMIC COMPUTER MODELING OF CONFINED MICROEXPLOSION

As we demonstrated above, plasma created by the rapid laser energy deposition in a focal volume attains the local thermodynamic equilibrium in time scale of the order of 1 ps. The process of plasma expansion into a cold solid on the larger time scales can be described in the frames of high-temperature hydrodynamics. The radiation hydrodynamics code "Chivas",[43] designed for numerical simulations of the laser-plasma interaction and the target compression for the inertial confinement fusion, has been used for the numerical simulations of the microexplosion. Chivas is a one-dimensional, two-temperature (electrons and ions) hydrodynamic code, which accounts for the electron and ion thermal transport, electron-ion coupling, and transient ionization. The ionization states and opacity data were calculated assuming a local thermodynamic equilibrium. The equation of state (EOS) implemented in the code (QEOS) is described in Ref. 44. Three parameters, the mass density $\rho_0=2.2$ g/cm^3, the bulk modulus $Y=75$ GPa, and the binding energy 3.16 J/mol (3.29 eV/atom), define the EOS for a glass. The main aims of the calculations were to reproduce the experimental observations: the absence of a void at low energy, the threshold for void formation, and the dependence of the void size on the deposited energy. The full set of these data was obtained for sapphire with the Young's modulus of 400 GPa. Therefore, we expect the calculations results for glass (sizes of void and laser-affected region) can be larger than those for sapphire by the factor $\sqrt[3]{400/75}=1.75$. The calculations were performed in the spherical geometry. We approximated the cylindrical region where the energy is deposited by an equivalent sphere of a radius r_{dep}. It was calculated from the known volume of the energy deposition: $V_{abs}=\pi r_{1/2}^2 l_{abs}=\frac{4}{3}\pi r_{dep}^3$. The energy in a range from 1 to 100 nJ was deposited homogeneously at $t=0$ in the spherical volume of radius $r_{dep}=0.13$ μm. Note that the energy density of 4.25 MJ/cm^3 in the volume V_{abs} (Sec. III H) corresponds to the deposited energy E_a of 39 nJ. At the absorbed energy of $E_a=1$ nJ, the initial pressure is comparable to the Young's modulus, therefore a void in glass can be formed at deposited energy >1 nJ.

Figure 6 shows the density and pressure profiles corresponding to the propagation of the shock and rarefaction waves for the case of absorbed energy of 50 nJ in the silica sample during the time period up to 20 ps. The instantaneous isochoric heating produces the average ionization $Z=4.83$ and the pressure P_0 of 2.6 TPa, which exceeds the bulk modulus more than 500 times. It is in good agreement with the simple estimate made above in Sec. III H ($P_0=2.7$ TPa and $n_e=3\times10^{23}$ cm^{-3}). The strong shock wave emerges at the outer surface of the energy deposition sphere, compressing material to a density twice of the initial one. Then, the

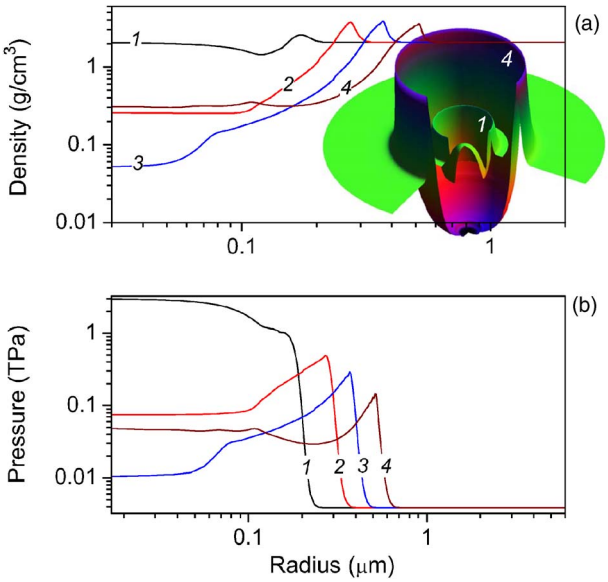

FIG. 6. (Color online) Density (a) and pressure (b) distributions behind the shock wave propagating in SiO_2 for the case of absorbed energy of 50 nJ. The results from the hydrodynamic code "Chivas" for the time moments of 1, 5, 10, and 20 ps (curves 1–4, respectively). The beginning of the void formation is clearly seen after the time of 5 ps. The inserts show the corresponding profiles in a linear scale.

pressure behind the shock front rapidly decreases with the distance and finally the shock transforms into the acoustic wave at $t=50$ ps. The spatial density profiles for the time moments up to 0.9 ns are shown in Fig. 7. The compression ratio δ at time of 1 ns reaches its asymptotic value of $\delta=1.1$ that qualitatively complies with the density of the amorphous layer retrieved from experiments, $\delta=1.14$. We note that the gas density in the central void region at 1 ns is above 0.1 g/cm^3. The calculated dependence of the cavity radius in SiO_2 on the absorbed energy can be interpolated by a simple power dependence

$$r_v \sim E_a^{0.42}\ \mu\text{m}, \tag{26}$$

where the absorbed energy is in nJ, which qualitatively complies with experimental dependence. Summing up we conclude that the hydrodynamic calculations predict the evolution of the laser-affected solid in qualitative agreement with the experimental data. The hydrodynamic simulations in the present model are valid during a few hundred ps until the material motion stops. Further simulations have to take into account the viscous dissipation and complicated processes of solidification. The more detailed description of solid-melt-vapor direct and reverse phase transitions is needed. The radiative losses and two-dimensional model should be implemented for more accurate description of microexplosion. These processes definitely affect the final state of a material cooled back to room temperature. Below we present a qualitative picture of phase transformations based on the calculated pressure and temperature profiles and on the literature data.

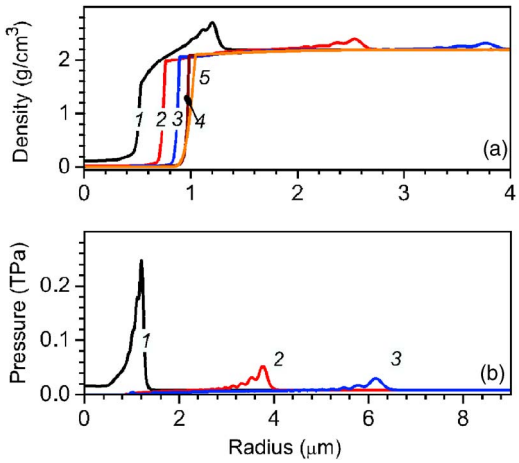

FIG. 7. (Color online) Density profiles (a) behind the shock wave for later time moments of 0.1, 0.3, 0.5, 0.7, and 0.9 ns (curves 1–5 respectively), and pressure profiles (b) for time moments of 0.1, 0.5, and 0.9 ns (curves 1–3, respectively), in a silica glass for the case of the absorbed energy of 50 nJ. The decay of the shock amplitude is clearly seen.

VI. PROPERTIES OF SHOCK-AND-HEAT-AFFECTED SOLID AFTER UNLOADING

Phase transformations in the quartz, silica, and glasses induced by strong shock waves have been studied for decades (see Refs. 41 and 45 and references therein). The pressure ranges for different phase transitions to occur under shock wave loading and unloading have been established experimentally and understood theoretically.[45] Quartz and silica convert to dense phase of stishovite (mass density 4.29 g/cm^3) in the range between 15 and 46 GPa. The stishovite phase exists up to a pressure of 77–110 GPa. Silica and stishovite melt at $P>110$ GPa, that is, in excess of the shear modulus for liquid silica ~10 GPa.

Dense phases usually transform into low-density phases (2.14–2.29 g/cm^3) when the pressure releases back to the ambient level. Numerous observations indicate a transition to an amorphous state upon the compression and decompression. An amorphous phase, which is denser than the crystalline silica, sometimes forms when unloading occurs from 15 to 46 GPa. The analysis of experiments shows that the pressure release and the reverse phase transition follows an isentropic path.

In studies of shock compression and decompression under the action of shock waves induced by explosives, the loading and release time scales are in the order of ~1–10 ns. The heating rate in the shock wave experiments is 10^3 K/ns, that is, the temperature rises to 10^3 K during 1 ns. In contrast, the peak pressure at the front of the shock wave driven by the laser [Fig. 6(b)] reaches the level of 10^3 GPa, that is, 100 times in excess of the pressure value necessary to induce structural phase changes and melting. Therefore, the region where the melting occurs is located very close to where the energy is deposited. The zones where structural changes and the transition to the amorphous state occur are located further away. The electron temperature in the energy deposition volume rises to 10^6 K during laser pulse time. This energy is

transferred to the atomic subsystem within the time of the order of 1 ps. This corresponds to the heating rate above 10^6 K/ps: four orders of magnitude larger than with conventional chemical explosives. The cooling time of a micron-sized heated region takes tens of microseconds. Supercooling of dense phases may occur if the quenching time is sufficiently short. A short heating and cooling time along with a small size of the area where the phase transition takes place can affect the rate of the direct and reverse phase transitions. In fact, phase transitions in these space and time scales have known very little.

The refractive index changes in a range of 0.05–0.45 along with protrusions surrounding the central void that were denser than silica were observed as a result of laser-induced microexplosion in a bulk of silica.[4] This is the evidence of formation of a denser phase during the fast laser compression and quenching; however, little is known of the exact nature of the phase.

Thus, we can conclude that a probable state of a laser-affected glass between void and shock stopping distance may contain amorphous material, that is denser, and with larger refractive index than the initial glass.

VII. SIMILARITY BETWEEN MICRO- AND MACROSCOPIC EXPLOSIONS

The microexplosion can be described solely in frames of an ideal hydrodynamic model if the heat conduction and other dissipative processes characterized by specific length scales can be ignored. The hydrodynamic equations contain five variables: the pressure, P; the density, ρ; the velocity, v; the distance, r; and the time, t. Three of them are independent, and the other two can be expressed through those three. The microexplosion can be characterized by the following independent parameters: the radius of the energy deposition zone, R_0; the initial deposited energy, E_0; and the initial density, ρ_0. Then the initial pressure is $P_0=E_0/R_0^3$ and the initial velocity is $v_0=(P_0/\rho_0)^{1/2}$. One can neglect energy deposition time and time for the energy transfer from electrons to ions (1 ps) in comparison to the hydrodynamic time of a few ns.

Then, the hydrodynamic equations can be reduced to set of ordinary equations with one variable, [41] $\xi=r/v_0t$, describing any hydrodynamic phenomena with the same initial pressure and density (velocity), but with the characteristic distance and time scales changed in the same proportion. When the energy of explosion increases, the space, R_0, and time scales are increased accordingly to $R_0=(E_0/P_0)^{1/3}$ and $t_0=R_0/v_0$. The similarity laws of hydrodynamics suggest that the microexplosion in sapphire ($E_0=100$ nJ, $\rho_0\sim 4$ g/cm^3, $R_0=0.15$ μm, $t_0=5.5$ ps) is a reduced copy of a macroscopic explosion that produces the same pressure at the same initial density, but with the distance and time scales changed in accordance with the above formulas. For example, the energy 10^{14} J (that is equivalent to 25 000 tons of a high explosive) released in a volume of 4 m^3 ($R_0=1.59$ m) exerts the same pressure as the laser-induced microexplosion insapphire; $P_0=12.5$ TPa in the time scale of 20 μs. Thus, exactly the same physical phenomena occur at the scale 10^7 times different in space and in time and 10^{21} times different in energy. Therefore all major hydrodynamic aspects of the powerful macroscopic explosion can be reproduced in laboratory table-top experiments.

VIII. CONCLUSIONS

The presented experimental and theoretical studies of intense laser beam interaction inside a transparent solid allow drawing the following conclusions. A transparent solid is converted to plasma by the action of a single fs pulse that resulted in the micrometer-sized void formation inside a bulk of a solid. The following stages of this transformation were identified.

First, the laser beam has been tightly focused inside of a transparent solid (up to 50 μm depth, much larger than the laser wavelength) into a focal volume ~ 0.3 μm^3. The high-intensity laser field ($\sim 10^{14}$ W/cm^2) inside the focal volume swiftly transforms a material into a plasma. The interplay between electron avalanche and the multi-photon ionization is the major factor leading to the optical breakdown in a transparent solid. That results in dramatic modifications of optical properties of a material followed by a strong laser absorption and a high concentration of energy in the absorption volume that decreases down to 0.15 μm^3. As a result, a huge absorbed energy density of 2.7 MJ/cm^3 has been created in the absorption volume. The pressure almost three orders of magnitude higher than the strength of material has been created.

The strong expanding shock wave was generated to compress the material surrounding the absorption volume and

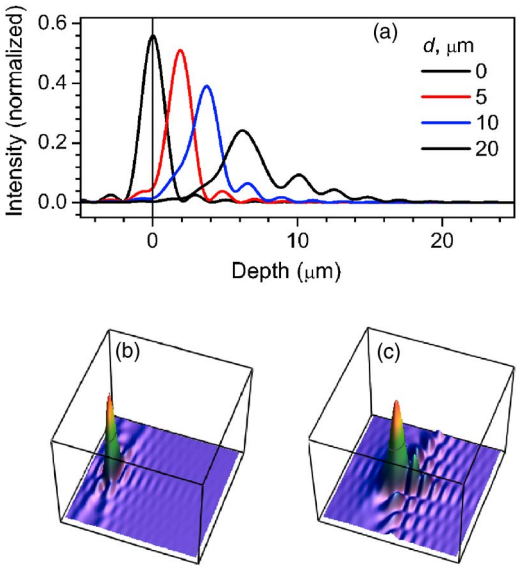

FIG. 8. (Color online) (a) Axial intensity distributions distorted by the spherical abberation for focusing of a *plane wave* by an objective lens of numerical aperture $NA=1.35$ ($\alpha=63^\circ$) from immersion oil, $n=1.515$, into sapphire, $n=1.7$, at different depth [aimed depth, d, is shown in (a); $d=0$ corresponds to the abberation-free focusing]. The wavelength of the light beam was $\lambda=800$ nm. The apodization function obeys a sine condition $P(\theta)=\sqrt{\cos(\theta)}$. (b), (c) The normalized 3D point spread function [same as in (a)] at 0 and 20 μm depth, respectively [Eq. (A5)]. Lateral and axial spans of 3D-PSF plots were 4 and 30 μm, respectively.

simultaneously (due to mass conservation law) create a void in the focal volume center. The size of the void and the amorphous material around has been observed and measured by means of high-resolution electron microscopy giving a void size of 200–500 nm.

These phenomena were simulated by using the radiative hydrodynamic code with a real equation of state. The predicted void size and the size of the laser-affected area are in qualitative agreement with the experiments and simpler analytic models. On the basis of these studies one can predict the size of the void produced by the single and multiple laser pulses with a reasonable accuracy. Moreover, since the void size and the damaged area characteristics are very sensitive to the EOS parameters, the experimental data could be used for correction of the existent EOS in the domain of phase transitions. This might bring new important results for many applications including the fusion research.

Thus, the possibility to create the extreme conditions (temperature rise rate $\sim 10^{18}$ K/s, pressure up to several TPa, temperature ~ 100 eV) by a single laser pulse in controlled laboratory conditions has been demonstrated, opening a field for studying the extreme states of matter or unusual material transformations. These studies also open a broad field of applications in the photonics (three-dimensional optical memories and arrangements of waveguides).

There are still many interesting problems to be resolved. It is very difficult to detect and calculate how the laser-matter interaction proceeds in three-dimensional space during the pulse and after the pulse end. This includes the relation between an axially symmetric focused beam and the real distribution of the absorbed energy density, electron density, temperature, and pressure. We do not know yet the exact phase state and the distribution in space of the laser-modified material, which will be important for the formation of a three-dimensional photonic crystal.

The studies of tightly focused lasers inside the transparent solid encompass a very exciting field for both applied and fundamental science with many problems to be uncovered. For example, the fundamental problem of phase transitions in conditions when the temperature (pressure) in a volume less than a cubic micron rises and falls in a few picoseconds is poorly understood. The rate of rise of temperature in these conditions $>10^{16}$ K/s is impossible to achieve by any other means. In such a condition new states of matter are most probably created. From the viewpoint of applications the question arises of how much smaller the size of the void can be made: That is directly relevant to the possible application of microexplosion for the memory storage. One cannot exclude that fundamental and applied problems are closely interrelated: the formation of a new phase in a zone close to the peak intensity allows, in principle, the formation of a diffractive structure whose size is much smaller than a radius of a focal spot.

ACKNOWLEDGMENTS

E.G.G. and B.L.-D. gratefully acknowledge the support of the Australian Research Council.

APPENDIX A: LASER INTENSITY DISTRIBUTION IN A FOCAL DOMAIN

A plane wave that is focused by a lens creates the axially symmetric intensity distribution, the point spread function (PSF), at the focus.[11] The PSF is given in the focal plane by the same expression as for diffraction of a plane wave on a round aperture. We take the radius of the Airy disk (the first minimum of PSF), w_0, as a beam waist (radius). The plane wave can be focused to the diffraction limit, which depends on the focusing angle θ (a half of the focusing cone angle). It is customary to define the numerical aperture of the lens $\mathrm{NA}=n\times\sin\theta$ with n being the refractive index at the focus. Then the waist of the focal spot is given by

$$w_0 = \frac{0.61\lambda_0}{\mathrm{NA}}. \tag{A1}$$

Here, the wavelength λ_0 should be changed to λ_0/n when focus is placed inside media of index n. When abberations are not considered, the NA is the same for focusing inside material or in air ($n_{air}=1$). This is because from Snell's law $n_{air}\sin\theta_{air}=n_m\sin\theta_m$. Since the effective wavelength is shorter by n times inside material of index n, the focal spot is, accordingly, smaller by factor n [Eq. (A1)].

The Gaussian beam/pulse when focused has no minimum in the focal intensity distribution. So, it is necessary to define the intensity level at which to measure the lateral and axial cross sections of the focus. Since similar total energy is enclosed within Airy disk (83%) of the plane wave's PSF and within a $1/e^2$ envelope (86%) of the Gaussian profile it is usually adopted that the focal spot size diameter given by Eq. (A1) defines the focal spot of the Gaussian beam/pulse as well. The length of the waist of a Gaussian pulse/beam, a doubled Rayleigh length, is given by

$$2z_R = 2\frac{\pi w_0^2}{\lambda_0}n. \tag{A2}$$

Intensity is decreased twice, to a 0.5-level from that at the minimum waist, at distance z_R; the waist is $w_0(z_R)=\sqrt{2}w_0$.

In order to calculate a lateral cross-section of a Gaussian intensity, $I(r)=I_0\exp-2(r/w_0)^2$, distribution at the 0.5 level (FWHM), and the measure at $1/e^2$ level, the waist [Eq. (A1)] should be multiplied by a factor $\sqrt{\ln 2/2}=0.589$: hence, $r_{1/2}=\sqrt{\ln 2/2}w_0$ at which $I(r_{1/2})=I_0/2$. The volume of the focal spot where the normalized intensity is higher than the 0.5 of its maximum value at the waist is enclosed in a cylinder, which has diameter $r_{1/2}$ and length $2z_R$ [by use of Eqs. (A1) and (A2)]:

$$V_{1/2} = 2z_R\pi r_{1/2}^2 = 2z_R S_{1/2} = 0.947\frac{\lambda_0^3}{NA^4}n, \tag{A3}$$

where $S_{1/2}=0.405\frac{\lambda_0^2}{NA^2}$ is the focal spot area. Equation (A3) was used to calculate the focal volume. It should be noted that this expression is approximate, since the actual laser beams/pulses are neither plane waves nor Gaussian.

1. Spherical abberation

The primary source of distortions of the focal light intensity distribution, the point spread function (PSF), is

TABLE I. The ionization potentials, J_Z (in eV), for the silicon and oxygen from Ref. 47 (number of electrons per state is given in parantheses).

Electron state	1s	2s	2p	3s	3p
Si	1844(2)	154(2)	104(6)	13.46(2)	8.15(2)
O	538(2)	28.5(2)	13.6(4)	…	…

due to spherical abberation for the right angle incidence. It is increasingly significant for tight focusing using a high-NA optics. The spherical abberation appears when light traverses the boundary between materials of different dielectric constant and increases with the depth of focus, d, according to[46]

$$\Phi(\theta_1,\theta_2,d) = -kd[n_1\cos(\theta_1) - n_2\cos(\theta_2)], \qquad \text{(A4)}$$

where $n_{1,2}$ and $\theta_{1,2}$ are the refractive indexes and angles of the side rays along the light propagation and $k=2\pi/\lambda$ is the wavevector in vacuum. The focal intensity distribution, the point spread function (PSF), in cylindrical coordinates, r,z, in the case of scalar Debye theory is given by[46]

$$I_s(r_2,z_2,\theta_1,\theta_2,d) = \left| \int_0^{\alpha} P(\theta_1)\sin(\theta_1)[t_s + t_p\cos(\theta_2)]J_0(k_1 r_1 n_1 \sin(\theta_1))\exp[- i\Phi(\theta_1,\theta_2,d) - ik_2 z_2 n_2\cos(\theta_2)]d\theta_1 \right|^2, \qquad \text{(A5)}$$

where $t_s(\theta_1)=2\sin(\theta_2)\cos(\theta_1)/\sin(\theta_1+\theta_2)$ and $t_p = 2\sin(\theta_2)\cos(\theta_1)/[\sin(\theta_1+\theta_2)\cos(\theta_1-\theta_2)]$ are the Fresnel coefficients for s- and p-polarizations, respectively; NA $=n_1\sin(\alpha)$ is the numerical aperture of objective lens, $P(\theta_1) = \sqrt{\cos(\theta_1)}$ is the apodization function obeying the sine condition (the commercial objective lenses are designed to satisfy the sine condition), and $J_0(\cdots)$ is the zeroth-order Bessel function of the first kind. Equation (A5) is visualized in Fig. 8 for irradiation of sapphire at our experimental conditions. By changing the divergence of the laser beam the spherical aberration can be minimized and an aberration-free focusing can be achieved at a fixed depth within a 5–100 μm range.

TABLE II. Ionization energies Q_Z (in eV) for the silicon and oxygen.

Z_O, Z_{Si}	1	2	3	4	5	6	7	8
Q_Z^{Si}	8.15	16.3	29.76	43.2	147.2	251.2	355	459
Q_Z^{O}	13.6	27.2	40.8	54.4	82.9	111.4	649.4	…
$Q_Z^{Si}+2Q_Z^{O}$	35.35	70.7	111.3	152	313	474	1653.8	…

APPENDIX B: DELIVERY OF THE LASER BEAM INSIDE A SOLID: LIMITATIONS IMPOSED BY THE SELF-FOCUSING

The power in a laser beam aimed to deliver the energy inside a bulk transparent solid should be kept lower than the self-focusing threshold for the medium. The critical value for the laser beam power depends on the nonlinear part of refractive index, n_2 ($n=n_0+n_2I$) as follows:[12]

$$p_{cr} = \frac{\lambda^2}{2\pi n_0 n_2}. \qquad \text{(B1)}$$

The beam self-focusing begins when the power in a laser beam, p_0, exceeds the critical value, $p_0 > p_{cr}$. The Gaussian beam under the above condition self-focuses after propagating along the distance, L_{sf}:[12]

$$L_{sf} = \frac{2\pi n_0 r_{min}^2}{\lambda}\left(\frac{p_0}{p_{cr}} - 1\right)^{-1/2}. \qquad \text{(B2)}$$

For example, in a fused silica ($n_0=1.45$; $n_2=3.54\times10^{-16}$ cm^2/W) and for $\lambda=1$ μm, the critical power comprises 3 MW. Assuming $p_0=2p_{cr}$ and $r_{min}\sim\lambda$, one estimates the self-focusing distance to be 9λ. Therefore, one can obtain the intensities above 10^{13} W/cm^2 in the focal plane and stay below the self-focusing threshold by using high-aperture optics.

APPENDIX C: IONIZATION LOSSES IN SILICA

One can estimate the degree of ionization and losses on the basis of data from Table I, which are summarized in Table II.

APPENDIX D: MATERIAL AND OPTICAL PROPERTIES OF STUDIED SOLIDS

Table III.

TABLE III. Material and optical properties of studied solids.

Solid	Refractive index[a] (n)	Young modulus (GPa)	Formation threshold[b] (nJ) Amorphous/Void	Depth (μm)	n_2 (cm^2/W)	Mass density (g/cm^3)
Sapphire	1.75	400	21/35	20	3×10^{-16} (Ref. 48)	3.89
Viosil	1.47	75	13/30	30	3.5×10^{-16}	2.2
Polystyrene	1.55	3.5	6/11	10	-9.3×10^{-9} (Ref. 49)	1.05

[a]The approximate values for 700–900 nm wavelengths. Refractive index of immersion oil was approximately 1.51.

[b]Thresholds have been measured in the present study by the best fit procedure shown in Fig. 3. The threshold value "amorphous" marks the optically recognizable breakdown threshold in the viosil and polystyrene; this threshold corresponds to the amorphisation onset in the case of crystalline sapphire.

*Electronic address: EGG@velocitynet.com.au
†Electronic address: Saulius@es.hokudai.ac.jp
‡Electronic address: Misawa@es.hokudai.ac.jp

[1] S. Juodkazis, A. V. Rode, E. G. Gamaly, S. Matsuo, and H. Misawa, Appl. Phys. B **B77**, 361 (2003).
[2] C. B. Schaffer, A. Brodeur, J. F. García, and E. Mazur, Opt. Lett. **26**(2), 93 (2001).
[3] H. Misawa, Electronics Weekly (UK) May 10, 3 (1995).
[4] E. N. Glezer, M. Milosavljevic, L. Huang, R. J. Finlay, T.-H. Her, J. P. Callan, and E. Mazur, Opt. Lett. **21**, 2023 (1996).
[5] M. Watanabe, H.-B. Sun, S. Juodkazis, T. Takahashi, S. Matsuo, Y. Suzuki, J. Nishii, and H. Misawa, Jpn. J. Appl. Phys., Part 2 **27**(12B), L1527 (1998).
[6] J. Qiu, K. Miura, H. Inouye, J. Nishi, and K. Hirao, Nucl. Instrum. Methods Phys. Res. B **141**, 699 (1998).
[7] H. Sun, Y. Xu, S. Juodkazis, K. Sun, M. Watanabe, S. Matsuo, H. Misawa, and J. Nishii, Opt. Lett. **26**(6), 325 (2001).
[8] S. Juodkazis, T. Kondo, V. Mizeikis, S. Matsuo, H. Misawa, E. Vanagas, and I. Kudryashov, in *ROC-Lithuania Bilateral Conf. Opoelectronics & Magnetic Materials (May 25–26 2002, Taipei, Taiwan) Proc.* (preprint:http://arXiv.org/abs/physics/0205025), pp. 27–29.
[9] E. G. Gamaly, A. V. Rode, B. L. Davies, and V. T. Tihonchuk, Phys. Plasmas **9**, 949 (2002).
[10] B. Luther-Davies, A. V. Rode, N. Madsen, and E. G. Gamaly, Opt. Eng. **44**, 051102 (2005).
[11] M. Born and E. Wolf, *Principles of Optics*, 7th ed. (Cambridge University Press, Cambridge, 2003).
[12] S. Akhmanov, V. Vyspoukh, and A. Chirkin, *Optics of Femtosecond Laser Pulses* (Nauka, Moscow, 1988).
[13] S. Matsuo and H. Misawa, Rev. Sci. Instrum. **73**, 2011 (2002).
[14] S. Juodkazis, T. Kondo, S. Dubikovski, V. Mizeikis, S. Matsuo, and H. Misawa, in *Int. Conf. Advanced Laser Technologies, ALT-2002 (Sept. 15-20 2002, Adelboden, Switzerland) SPIE Proc. 5147*, edited by H. P. Weber, V. I. Konov, and T. Graf (SPIE, Bellingham, WA, 2003), pp. 226–235.
[15] P. O'Shea, M. Kimmel, X. Gu, and R. Trebino, Opt. Lett. **26**, 932 (2001).
[16] S. Juodkazis, Y. Tabuchi, T. Ebisui, S. Matsuo, and H. Misawa, in *Advanced Laser Technologies (Sept. 10-15, 2004, Rome & Frascati, Italy), SPIE Proc. vol. 5850*, edited by I. A. Shcherbakov, A. Giardini, V. I. Konov, and V. I. Pustovoy (SPIE, Bellingham, WA, 2005), pp. 59–66.
[17] S. Juodkazis, K. Nishimura, H. Misawa, T. Ebisui, R. Waki, S. Matsuo, and T. Okada, Adv. Mater. (Weinheim, Ger.) **18**, 1361 (2006).
[18] A. Dubietis, E. Gaizauskas, G. Tamosauskas, and P. Di Trapani, Phys. Rev. Lett. **92**, 253903 (2004).
[19] E. Gaižauskas, E. Vanagas, V. Jarutis, S. Juodkazis, V. Mizeikis, and H. Misawa, Opt. Lett. **31**(1), 80 (2006).
[20] C. W. Carr, M. D. Feit, J. J. Muyco, and A. M. Rubenchik, in Optical Materials for High-Power Lasers, Proc. SPIE **5647**, 532 (2004).
[21] H. Misawa, H.-B. Sun, S. Juodkazis, M. Watanabe, and S. Matsuo, in *Laser applications in microelectronics and optoelectronic manufacturing V, LASE (Jan. 22-28, 2000, San Jose, USA) SPIE Proc. 3933*, edited by H. Helvajian, K. Sugioka, M. C. Gower, and J. J. Dubikowski (SPIE, Bellingham, WA, 2000), pp. 246–260.
[22] L. Landau and E. Lifshitz, *Electrodynamics of Continuous Media* (Pergamon, Oxford, 1984).
[23] Y. P. Raizer, *Laser-induced Discharge Phenomena* (Consultant Bureau, New York, 1977).
[24] E. Yablonovitch and N. Bloembergen, Phys. Rev. Lett. **29**, 907 (1972).
[25] D. Fradin, N. Bloembergen, and J. Letellier, Appl. Phys. Lett. **22**, 635 (1973).
[26] D. Arnold and E. Cartier, Phys. Rev. B **46**, 15102 (1992).
[27] D. Du, X. Liu, G. K. J. Squier, and G. Mourou, Appl. Phys. Lett. **64**, 3071 (1994).
[28] B. C. Stuart, M. D. Feit, A. M. Rubenchick, B. W. Shore, and M. D. Perry, Phys. Rev. Lett. **74**, 2248 (1995).
[29] D. von der Linde and H. Schuler, J. Opt. Soc. Am. B **13**(1), 216 (1996).
[30] K. Miura, J. Qiu, H. Inouye, and T. Mitsuyu, Appl. Phys. Lett. **71**, 3329 (1997).
[31] P. Pronko, P. VanRompay, C. Horvath, F. Loesel, T. Juhasz, X. Liu, and G. Mourou, Phys. Rev. B **58**, 2387 (1998).
[32] M. Lenzner, J. Kruger, S. Sartania, Z. Cheng, C. Spielmann, G. Mourou, W. Kautek, and F. Krausz, Phys. Rev. Lett. **80**, 4076 (1998).
[33] A. C. Tien, S. Backus, H. Kapteyn, M. Murname, and G. Mourou, Phys. Rev. Lett. **82**, 3883 (1999).
[34] L. Sudrie, A. Couairon, M. Franco, B. Lamouroux, B. Prade, S. Tzortzakis, and A. Mysyrovicz, Phys. Rev. Lett. **89**, 186601 (2002).
[35] C. W. Carr, H. B. Radousky, A. M. Rubenchik, M. D. Feit, and S. G. Demos, Phys. Rev. Lett. **92**, 087401 (2004).
[36] Y. Il'inski and L. Keldysh, *Electromagnetic Response of Material Media* (Plenum, New York, 1994).
[37] K. Eidmann, J. Meyer-ter-Vehn, T. Schlegel, and S. Huller, Phys. Rev. E **62**, 1202 (2000).
[38] J. R. Oppenheimer, Phys. Rev. **31**, 66 (1928).
[39] L. V. Keldysh, Zh. Eksp. Teor. Fiz. **47**, 1945 (1964) [Sov. Phys. JETP **20**, 1307 (1965)].
[40] J. R. Penano, P. Sprangle, B. Hafizi, W. Manheimer, and A. Zigler, Phys. Rev. E **72**, 036412 (2005).
[41] Y. B. Zel'dovich and Y. P. Raizer, *Physics of Shock Waves and High-Temperature Hydrodynamic Phenomena* (Dover, Mineola, NY, 2002).
[42] W. L. Kruer, *Physics of Laser Plasma Interactions* (Addison-Wesley, New York, 1988).
[43] S. Jacquemot and A. Decoster, Laser Part. Beams **9**, 517 (1991).
[44] R. More, K. Warren, D. Young, and G. Zimmerman, Phys. Fluids **31**, 3059 (1988).
[45] S. Luo, T. Arens, and P. Asimov, J. Geophys. Res. **108**, 2421 (2003).
[46] M. Gu, *Advanced Optical Imaging Theory* (Springer, Berlin, 1999).
[47] L. A. Vanshtein and V. Shevel'ko, *Structure and Characteristics of Ions in Hot Plasma* (Nauka, Moscow, 1986) (in Russian).
[48] A. M. F. Y. I. Nikolakakos, J. S. Aitchison, and P. W. E. Smith, Opt. Lett. **29**, 602 (2004).
[49] A. Miniewicz, S. Bartkiewicz, J. Sworakowski, J. A. Giacometti, and M. M. Costa, Pure Appl. Opt. **7**, 709 (1998).